

<https://doi.org/10.1038/s43247-025-02147-x>

# Anthropogenic sulfate-climate interactions suppress dust activity over East Asia

Check for updates

Xiaoning Xie<sup>1,2</sup>✉, Gunnar Myhre<sup>3</sup>, Huizheng Che<sup>4</sup>, Feng Wu<sup>1</sup>, Jianing Guo<sup>1</sup>, Zhengguo Shi<sup>1</sup>, Xinzhou Li<sup>1</sup>, Xiaodong Liu<sup>1,5</sup> & Yangang Liu<sup>6</sup>✉

Observational evidences indicate a significant decline in dust storm frequencies over the East Asian arid-semiarid region during recent decades, which creates a strong contrast with a great increase in sulfate emissions over monsoonal Asia. However, the causes for decline of dust activities are still controversial. Through conducting a set of idealized sensitivity experiments of regional aerosol perturbations, here we show that anthropogenic sulfate aerosols over monsoonal Asia remarkably suppress the regional dust activities over East Asia. Southward shift of Asian westerly jet stream induced by sulfate aerosols results in increasing precipitation and weakening surface wind speeds over the arid-semiarid region, thereby suppressing local dust emission fluxes. Further, the latest Sixth Coupled Model Intercomparison Project simulations indicate that anthropogenic aerosols partly drive the recent weakening in regional dust activities and that future change of regional dust activities will likely depend on emissions scenarios of Asian anthropogenic aerosols and greenhouse gases.

As a natural phenomenon, dust activity mainly induced by strong winds from arid-semiarid lands has a remarkable impact on atmospheric environment and land-to-ocean ecosystems through triggering severe dust storms and global/regional climate through dust-radiation and dust-cloud-radiation interactions<sup>1–4</sup>. Due to existence of the Taklamakan and Gobi deserts over East Asia (EA), dust storms occur frequently throughout the year, with most occurring during spring<sup>5–7</sup>. Observational results show a weakened dust activity over EA with Northwest China as its core since the late 1970s<sup>8–10</sup>.

Previous studies of diagnostic analysis have linked the EA weakened dust activities to remote and local climate changes associated with global warming caused by human-produced greenhouse gases (GHGs)<sup>8,9,11–13</sup>. One mechanism proposes that the amplified Arctic warming results in a reduction of the meridional temperature gradient and surface wind speeds over mid-latitudes of the North Hemisphere, which therefore decreases EA dust activities<sup>8,9,13,14</sup>. Another proposed mechanism is related to increased local precipitation over the EA arid-semiarid region through enhancing convective instability, increasing transport of atmospheric water vapor, and accelerated melting of snow and glaciers over high-mountain Asia<sup>15–17</sup>. The precipitation increase enhances local soil moisture and vegetation coverage, which in turn weakens EA dust storm events<sup>11,14,18</sup>.

Anthropogenic aerosols have been suggested as an important driver of global/regional climate change, contributing the second-largest forcing in earth-system models relative to GHGs<sup>19–21</sup>. Over monsoonal Asia such as eastern China and Indian subcontinent, anthropogenic aerosols have dramatically increased over recent decades<sup>22–25</sup>. Many previous modeling studies suggested that increased anthropogenic sulfate aerosols over the Asian polluted regions significantly reduce the South Asian monsoon and East Asian monsoon through altering the land-sea thermal contract and cloud microphysical properties<sup>26–29</sup>, and enhance the summer precipitation over the EA arid-semiarid region through altering the Asian westerly jet stream<sup>30</sup>. However, relatively little attention has been paid to how the feedbacks of sulfate-climate interaction in the Asian polluted regions influence on the EA dust activities. Here, using a global climate model (GCM) with dust cycle processes, we perform a series of idealized sensitivity experiments with Asian sulfate aerosols to investigate the sulfate-induced impact on EA dust activities. We quantify the changes of EA dust activities induced by Asian sulfate and examine possible physical mechanisms related to regional climate change. We further utilize multi-model simulations from the Precipitation Driver and Response Model Intercomparison Project (PDRMIP) to identify the climatic causes of the weakened EA dust activities and the connection to sulfate emissions in the polluted regions over Asia.

<sup>1</sup>State Key Laboratory of Loess Science, Institute of Earth Environment, Chinese Academy of Sciences, Xi'an, China. <sup>2</sup>CAS Center for Excellence in Quaternary Science and Global Change, Xi'an, China. <sup>3</sup>CICERO - Center for International Climate Research, Oslo, Norway. <sup>4</sup>State Key Laboratory of Severe Weather & Key Laboratory of Atmospheric Chemistry of CMA, Chinese Academy of Meteorological Sciences, Beijing, China. <sup>5</sup>University of Chinese Academy of Sciences, Beijing, China. <sup>6</sup>Environmental and Climate Sciences Department, Brookhaven National Laboratory, Upton, NY, USA. ✉e-mail: [xnxie@ieecas.cn](mailto:xnxie@ieecas.cn); [lyg@bnl.gov](mailto:lyg@bnl.gov)

## Results and Discussion

### Observational relationships between dust activity and sulfate AOD

Due to existence of Taklamakan and Gobi deserts over the East Asian arid-semiarid regions, dust storms occur frequently throughout the whole year, with most occurring in spring, which results in a large amount of desert dusts emitted into atmosphere and transported to the downwind regions including the Chinese Loess Plateau and the Pacific Ocean<sup>5-7</sup>. According to station observations from the China Meteorological Administration (CMA), Supplementary Fig. 1 displays a spatial distribution of observed annual dust storm days over EA on average over the time period from 1979–1988. In contrast to eastern China with the low frequency of dust activities, the CMA site observations show much more extreme dust events over the EA arid-semiarid region, which is much >10 days climatologically. In view of seasonal means, it shows large seasonal variations of dust activity. It indicates that dust storms occur most frequently in MAM (March–May) and followed by JJA (from June to August) in Supplementary Fig. 1. During the period (1979–2013). It shows a substantial decrease in the EA dust activities across most of the EA arid-semiarid region in Fig. 1a. In addition, Fig. 1b further shows a significantly weakening trend in the dust storm frequency with -2.37 days per decade, approximately -29% per decade relative to 1979–1988. The EA weakened dust activity since the late 1970s is generally consistent with previous observational studies<sup>8-10</sup>.

Due to the population explosion and the rapid economic growth over monsoonal Asia during recent decades, anthropogenic aerosol emissions over the Asian polluted regions have dramatically increased<sup>22-25</sup>. The Modern-Era Retrospective analysis for Research and Applications, Version 2 (MERRA-2) is a long-term global reanalysis beginning in 1980, which assimilates aerosol observations and considers the aerosol-radiation-cloud interactions in the climate system<sup>31</sup>. Here, we used sulfate AOD data from the MERRA-2 Aerosol Reanalysis, instead of observational data. It shows an increasing trend of sulfate AOD over Asia during the recent period from 1980 to 2013 based on MERRA-2, especially over eastern China and Indian subcontinent (Fig. 1c). In the following subsection, we will examine the Asian sulfate aerosol effect on regional dust cycle to provide a possible causal

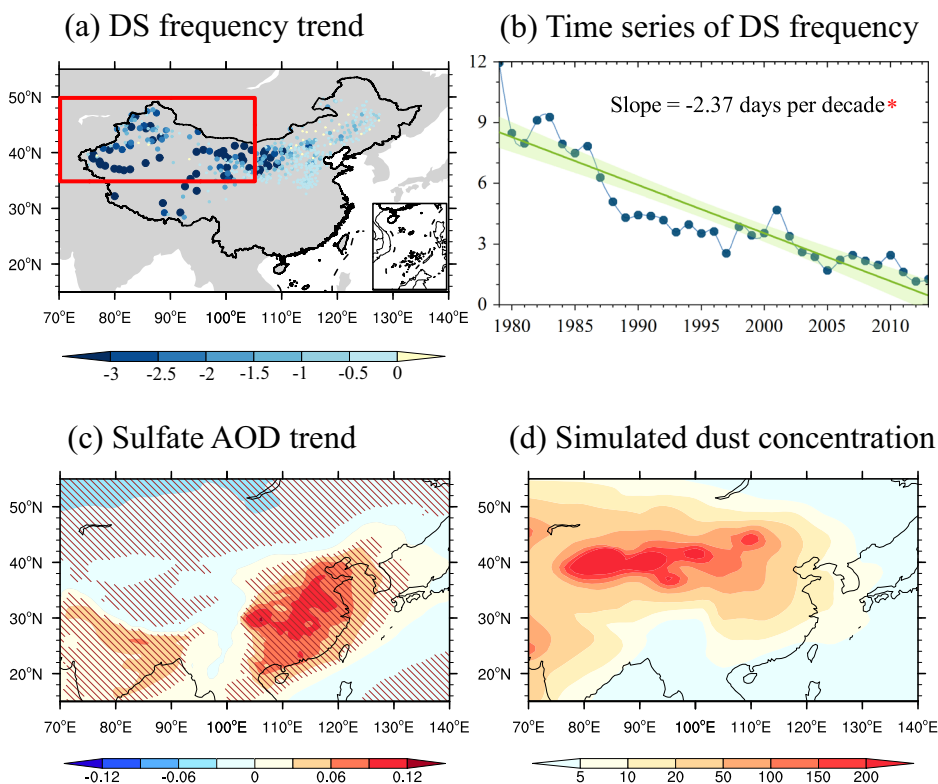
relationship between the Asian sulfate aerosols and dust activities during recent decades.

### Anthropogenic sulfate-induced change of EA dust activity

The CAM4-BAM simulates the spatial distribution of surface dust mass concentration annually on average (Fig. 1d). It shows that the dust surface mass concentration decreases rapidly from the arid-semiarid region (dust source region) to eastern China in CAM4-BAM, consistent with that of dust storm frequency in the CMA site observations in Supplementary Fig. 1. We further compare the simulated surface mass concentration, dust AOD, and sulfate AOD with the MERRA-2 reanalysis over Aisa, indicating that the model can mainly capture the spatial distribution of dust and sulfate aerosols (Supplementary Fig. 2). Additionally, we also show the regional precipitation and surface wind speeds (defined as 10-m wind speeds) including observations and model, which is closely related to the dust emission process. The model shows low precipitation and large surface wind speeds over the EA arid-semiarid region, consistent with observations in Supplementary Fig. 3.

Note that the World Meteorological Organization (WMO) defines a dust storm event as the visibility <1000 m in site observations. According to the observation manual prepared by WMO, the present weather code (ww) related to dust storms are 09, 30 ~ 35, and 98 in CMA station observations. Here, an extreme dust event (dust storm) is calculated from the daily surface mass concentration in the model. If the daily mean value of surface mass concentration is larger than the 95th percentile as a threshold for all the grids over the region with 70–105°E and 35–50°N during the simulated 20 years (almost 376  $\mu\text{g m}^{-3}$ ), it is defined as an extreme dust event (dust storm day). Note that the threshold defined in the model is much less than observational values (several thousand micrograms per cubic meter) from the northeast Asian dust storm events<sup>32</sup>. This underestimation is mainly because that the daily mean value is used to define the dust storm in the model, whereas the instantaneous value is taken every 5 min in observations<sup>32</sup>. In addition, we display seasonal variations of dust surface mass concentration (Supplementary Fig. 4a) and dust storm days (Supplementary Fig. 4b) for MAM, JJA, SON (September–November), and DJF (December–February), showing

**Fig. 1 | Observed trends of dust storm (DS) frequency and Asian sulfate AOD. a** Annual DS frequency trends (days per decade) over East Asia during 1979–2013 and **(b)** time series of annual DS frequency over the region with 70–105°E, 35–50°N (red box in a). **c** Sulfate AOD trends (per decade) from 1980–2013 based on the MERRA-2 Aerosol Reanalysis. **d** Simulated annual dust surface mass concentration ( $\mu\text{g m}^{-3}$ ) in CAM4-BAM. Red star in (b) and slanted lines in (c) indicate significance at the 95% confidence level by a standard *t*-test.



largest dust activities in the MAM season and followed by JJA, which is absolutely consistent with observational dust storm frequency (Supplementary Fig. 1).

To quantify the sulfate-induced effects on regional dust cycle, annual changes of the EA dust activities induced by increasing Asian sulfate aerosols are shown in Fig. 2. The differences between the sensitivity experiments (SULx2Asia, SULx5Asia, and SULx10Asia, see Methods) and Base experiment show a considerable decrease in the annual surface dust mass concentration based on Fig. 2a–c, which is statistically significant over the EA arid-semiarid region in SULx5Asia (Fig. 2b) and SULx10Asia (Fig. 2c). Annual percentage change in dust mass concentration considerably reduces from  $-1.7\%$  to  $-8.2\%$  (Fig. 2d). For extreme dust events, we further show a significant reduction of dust storm days in SULx2Asia (Supplementary Fig. 5a), SULx5Asia (Supplementary Fig. 5b), and SULx10Asia (Supplementary Fig. 5c). Compared with mean mass concentration, it shows a much larger percentage in extreme dust events from  $-2.5\%$  to  $-13.2\%$  in Fig. 2d. This implies that the change of extreme dust events is much more than that of mean mass concentration. Further analysis from probability density function (PDF) of daily mass concentration shows that increasing Asian sulfate aerosols decrease the frequency of dust storm events ( $>376 \mu\text{g m}^{-3}$ ) in Supplementary Fig. 6a and 6b, which reinforces the result of larger percentage in the decline of extreme dust events. These results related to surface mass concentration and extreme dust events mainly resulted from the considerably reduced dust emissions over the arid-semiarid region (Fig. 2d), also shown in Supplementary Fig. 7. Additionally, the reduction of dust AOD is shown in Supplementary Fig. 8, which is significant for SULx5Asia and SULx10Asia.

Relative changes in the EA dust activities are shown for four seasons in Supplementary Fig. 9. The substantial decreases in the surface mass concentration (Supplementary Fig. 9a), frequency of extreme dust events (Supplementary Fig. 9b), and dust emission flux (Supplementary Fig. 9c) are all evident for the four seasons including MAM, JJA, SON, and DJF. Largest magnitude of the sulfate-induced changes is shown during JJA for all the

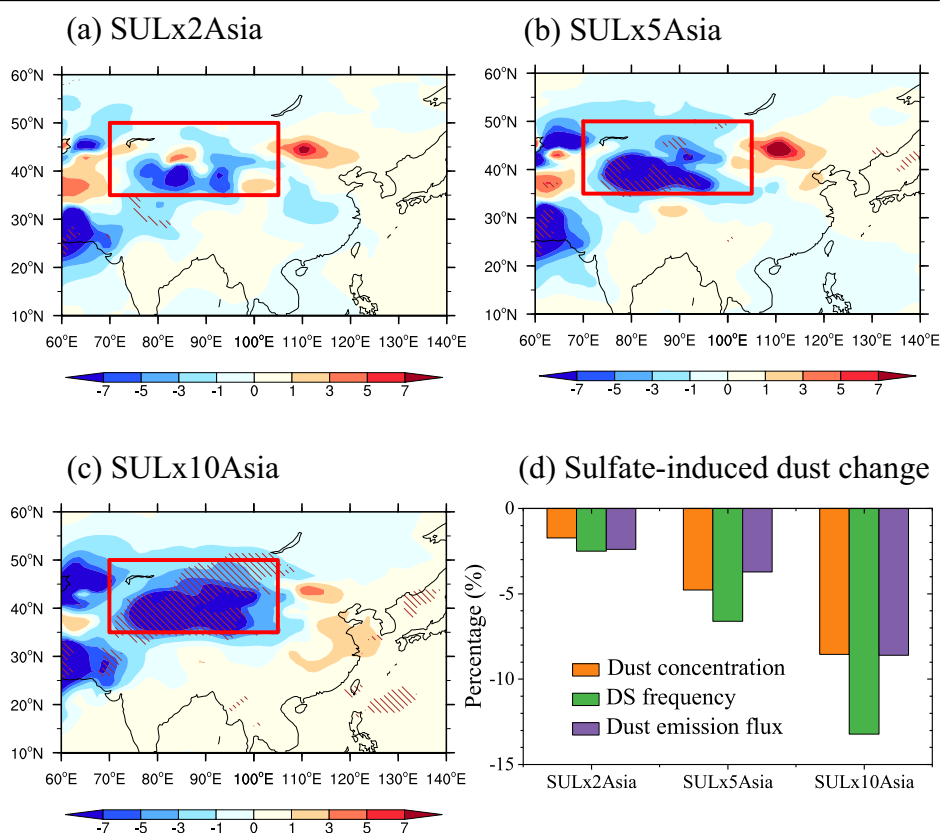
variables of the EA dust activity. Compared with mean surface mass concentration and dust emission flux, the change of extreme dust event frequency induced by sulfate aerosols has a larger percentage with  $-4.1\%$  (SULx2Asia),  $-13.3\%$  (SULx5Asia) and  $-25.3\%$  (SULx10Asia) during JJA. In general, our results show that increasing Asian sulfate aerosol considerably weakens the EA dust activity (especially extreme dust events) in annual and seasonal means with the largest change during JJA.

### Anthropogenic sulfate-induced climate feedbacks

To examine physical mechanisms of the significant weakening trend in EA dust activities, we analyze regional climate changes induced by increasing Asian sulfate aerosols during JJA. Here, the CAM4-BAM simulates the differences between SULx10Asia and Base experiments in JJA Asian westerlies, cloud amount, precipitation, and surface wind speeds, as summarized in Fig. 3. Supplementary Fig. 10a displays a spatial distribution of JJA westerly anomaly, showing a significant increase in westerlies at 200 hPa over the regions in the south of  $45^\circ\text{N}$  and a decrease at higher latitudes. Spatial pattern of change in westerlies indicates a considerable southward shift of Asian westerly jet stream (AWJS) with  $\sim 0.8$  degree between  $60^\circ\text{E}$ – $140^\circ\text{E}$ . Vertical profile of changes in westerlies also indicates a southward shift of AWJS (Supplementary Fig. 10b). A substantial increase in aerosol optical depth (Supplementary Fig. 10c) over the Asian polluted regions from SULx10Asia leads to local larger negative effective radiative forcing (Supplementary Fig. 10d), resulting in a significant cooling in mid-latitudes (Supplementary Fig. 10e) and spatial change of meridional temperature gradient (Supplementary Fig. 10f), in turn driving AWJS southward shift.

Asian sulfate-induced change of AWJS alters EA dust activities through influencing precipitation and surface wind speeds. The southward shift of AWJS leads to anomalous low-level southwesterly winds over low latitudes during JJA in Supplementary Fig. 11, which is favorable for the supply of water vapor from the Indian Ocean and moisture flux convergence over the EA arid-semiarid region<sup>30,33–35</sup>. Anomalous low-level circulations due to the AWJS shift significantly enhances regional cloud amount and

**Fig. 2 | Sulfate-induced changes in the dust activities over East Asia.** Annual changes in surface dust mass concentration ( $\mu\text{g m}^{-3}$ ) induced by (a) SULx2Asia, (b) SULx5Asia, and (c) SULx10Asia over East Asia in CAM4-BAM. **d** Annual percentage changes (%) in the surface dust mass concentration, dust storm (DS) frequency, and dust emission flux over the region with the red box in (a–c). Slanted lines in (a–c) indicate significance at the 95% confidence level and the red box indicates the region with  $70$ – $105^\circ\text{E}$  and  $35$ – $50^\circ\text{N}$ .



surface precipitation over the arid core region in Fig. 3, where the spatial distribution of cloud amount and surface precipitation are shown in Supplementary Fig. 12a and 12b, respectively. The increased regional precipitation in turn enhances soil moisture (Supplementary Fig. 12c) and decreases local dust emissions. The AWJS southward shift also leads to a

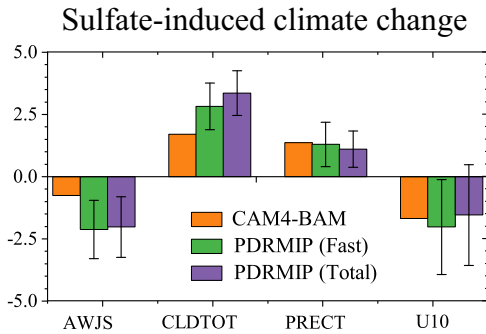


**Fig. 3 | Sulfate-induced climate changes in June–August (JJA) over East Asia.** Changes in the latitudinal position of JJA AWJS (degree), cloud fraction (CLDTOT, %), precipitation (PRECT,  $10^{-1}$  mm day $^{-1}$ ), and surface wind speeds (U10,  $10^{-1}$  m s $^{-1}$ ) over the arid core region (70°E–90°E, 35°N–50°N) induced by SULx10Asia in CAM4-BAM, compared with the PDRMIP fast and total responses. Error bars of the multi-model mean represent the standard deviation among the PDRMIP models.

**Table 1 | Sulfate-induced seasonal changes in regional climate over East Asia**

Season	AWJS	CLDTOT	PRECT	U10
MAM	-0.23	0.81	-0.01	-0.06
JJA	-0.76	1.70	0.14	-0.17
SON	-0.98	0.64	0.03	-0.15
DJF	0.08	0.64	-0.02	-0.12

Seasonal changes of the latitudinal position of AWJS (degree), cloud fraction (CLDTOT, %), precipitation (PRECT, mm day $^{-1}$ ), and surface wind speeds (U10, m s $^{-1}$ ) over the arid core region (70°E–90°E, 35°N–50°N) induced by SULx10Asia in CAM4-BAM.

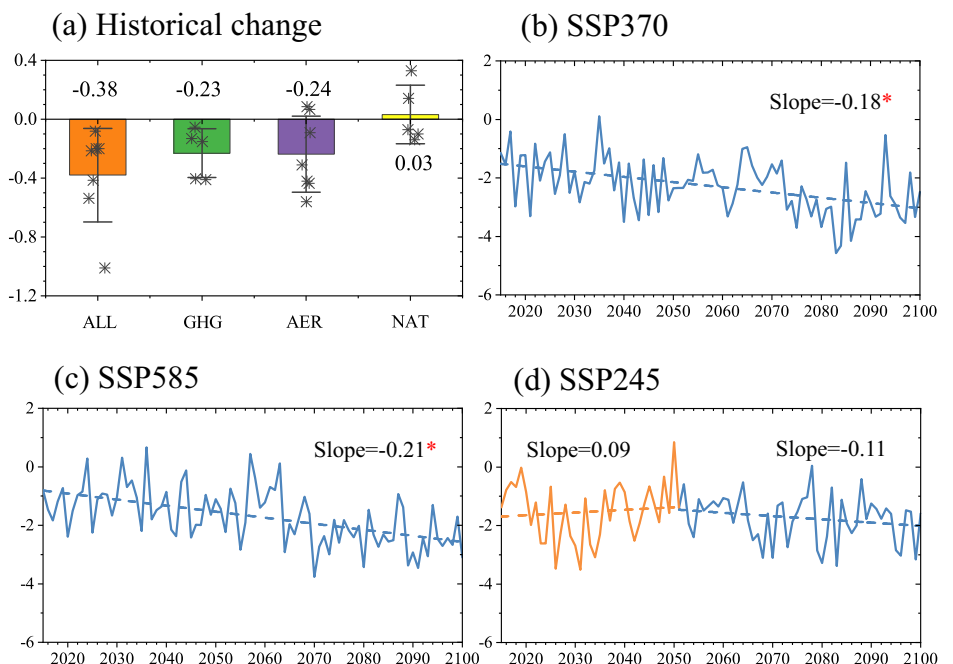
change of westerlies from high levels to low levels over mid-high latitudes, affecting a long-range transport to the Pacific Ocean, and occasionally to North America<sup>36,37</sup>. The increased cloud amount associated with the dynamic processes reduces the sunlight incident upon the surface of the Earth (Supplementary Fig. 12d), in turn decreases the turbulent fluxes of sensible heat from the surface to the atmosphere (Supplementary Fig. 12e). This results in a decrease of surface wind speeds (Fig. 3 and Supplementary Fig. 12f) though reducing the turbulent mixing within the planetary boundary layer, along with downward momentum transport to the surface, proposed in the previous studies<sup>38</sup>. The weakening in the surface wind speeds over the dust source regions reduces the amount of local dust emissions. Therefore, a combination of the increase in precipitation and the weakening in surface wind speeds due to increasing Asian sulfate aerosols suppresses the EA dust activities remarkably (Fig. 2). We also show the regional climate change during the four seasons induced by increasing Asian sulfate aerosols in Table 1. It shows a largest change in precipitation and surface wind speeds during JJA, which further supports the largest reduction in JJA dust cycle. Furthermore, decreased dust aerosols can enhance precipitation increase over the EA arid-semiarid region through dust-in-snow feedback mechanism<sup>39</sup> and dust-ice cloud interaction mechanism<sup>40</sup>, which then induces positive feedback between decreased dusts and increased precipitation. Note that the sulfate-induced climate feedbacks are absolutely based on the SULx10Asia experiment in CAM4-BAM, nonetheless the climate feedbacks from SULx2Asia and SULx5Asia show similar but smaller changes in AWJS, cloud amount and precipitation, and surface wind speeds (figures not shown).

**Comparisons with PDRMIP simulations**

The simulated climate feedbacks in CAM4-BAM are further compared with the multi-model PDRMIP simulations (see Methods). Figure 3 shows the changes in the JJA AWJS position, cloud amount, precipitation, and surface wind speeds averaged over the arid core regions (70°E–90°E, 35°N–50°N) in CAM4-BAM compared with the PDRMIP forced SST simulations and fully coupled simulations. It is evident in a southward-shifted AWJS, increased cloud amount, and precipitation, as well as weakened surface wind speeds from both the PDRMIP fast and total responses, which all supports the climate feedbacks of increasing Asian sulfate from CAM4-BAM. Furthermore, it shows similar values for fast and total responses in the AWJS southward shift in the PDRMIP simulations with  $-2.12 \pm 1.17$  degree (fast)

**Fig. 4 | Historical change and future projection of dust emission fluxes over East Asia in CMIP6.**

**a** The linear trend of EA dust emission fluxes ( $10^{-10}$  kg m $^{-2}$  s $^{-1}$  per decade) for ALL, GHG, aerosol (AER), and natural forcing simulations (NAT) in DAMIP over the region with 70–105°E and 35–50°N during the historical period (1979–2014). Time series of EA dust emission flux anomaly in multi-model ensemble ( $10^{-10}$  kg m $^{-2}$  s $^{-1}$ ) in **(b)** SSP370, **(c)** SSP585, and **(d)** SSP245 from 2015 to 2100, relative to 1979–2014. Black stars in **(a)** indicate individual model results and error bars of the multi-model mean represent  $\pm 1$  standard deviation among the CMIP6 models and. Red stars in **(b–d)** represent significance at the 95% confidence level.



and  $-2.02 \pm 1.22$  degree (total), cloud amount increase with  $2.82 \pm 0.94\%$  (fast) and  $3.36 \pm 0.90\%$  (total), precipitation increase with  $0.13 \pm 0.09$  mm day<sup>-1</sup> (fast) and  $0.11 \pm 0.07$  mm day<sup>-1</sup> (total), and reduction of surface wind speeds with  $-0.20 \pm 0.19$  m s<sup>-1</sup> (fast) and  $-0.15 \pm 0.20$  m s<sup>-1</sup> (total), respectively. This indicates that the total climate responses including AWJS, cloud amount, precipitation, and surface wind speeds to Asian sulfate aerosols are dominated by the fast responses due to local atmospheric cooling whereas the slow climate responses due to SST feedbacks can be ignored.

In contrast to scattering aerosols such as sulfate aerosols, light-absorbing black carbon (BC) directly absorbs incoming short-wave radiation and warms local atmosphere, which has the potential global and regional impacts of climate change<sup>20,21</sup>. Based on the PDRMIP simulations from perturbed experiments of Asian BC aerosols, increasing Asian BC exerts a poleward shift of AWJS through enhancing local atmospheric heating at middle and high latitudes over Asia and reduces the surface precipitation over the EA arid-semiarid region<sup>30</sup>, which likely enhances local dust emission fluxes and dust activities over EA and partially offsets the effect of Asian sulfate aerosols.

### Individual effects from anthropogenic sulfate aerosols over EA and SA

To check individual effects of sulfate aerosols over EA and SA, we also conduct two additional experiments about 10-fold increase in the present-day sulfate emissions over EA (SULx10EAsia) and over SA (SULx10SAsia). Supplementary Fig. 13 displays the changes of annual AOD and surface dust mass concentration induced by SULx10EAsia and SULx10SAsia, respectively. It shows that the increase in sulfate aerosols (or AOD) over EA and SA both decrease the surface dust mass concentration over the arid region in Supplementary Fig. 13. Due likely to larger change in sulfate AOD over EA (Supplementary Fig. 13a and 13b), increasing sulfate aerosols over EA shows the significant and great reduction in surface dust mass concentration (Supplementary Fig. 13c) compared with the SA sulfate aerosols in Supplementary Fig. 13d. Since 2011, regional aerosol emission has been rapidly changing over Asia, showing an aerosol dipole pattern with a continuous increase over SA and a significant reduction over EA<sup>41</sup>. The impact of this Asian aerosol dipole pattern on the regional dust activities remains largely unknown and merits further investigation.

### Application to historical and future trends of East Asian dusts

To further quantify relative contributions of different external drivers to dust activities over EA, we analyze historical trends of dust emission fluxes using the Detection and Attribution Model Intercomparison Project (DAMIP) in CMIP6<sup>42,43</sup>. Previous studies show that the CMIP6 models can mainly capture the spatial distribution seasonal cycles of dust emissions<sup>44–46</sup>. Here, we used the historical all forcing simulations including all natural and anthropogenic forcings and three single forcing simulations including include GHG, anthropogenic aerosol, and natural forcing based on nine GCMs in Supplementary Table 1. For the all forcing simulations in Fig. 4a, the multi-model mean shows a decreasing trend of dust emission fluxes over EA with  $-0.38 \times 10^{-10}$  kg m<sup>-2</sup> s<sup>-1</sup> per decade (approximately  $-2.3\%$  per decade) during 1979–2014, far less than the observed decreasing trend of dust storm frequency (Fig. 1b). GHGs emitted by human activities are a potential driver of 20th century climate change, several studies of diagnostic analysis have attributed the EA weakened dust activities to local and remote climate change associated with global warming induced by GHGs<sup>8,9,11–13</sup>. The results of the diagnosis analyses are confirmed by the GHG forcing simulations with a decreasing trend of  $-0.23 \times 10^{-10}$  kg m<sup>-2</sup> s<sup>-1</sup> per decade in Fig. 4a (all the GCMs have negative trends). Compared to GHGs, the aerosol forcing simulations show a similar trend of  $-0.24 \times 10^{-10}$  kg m<sup>-2</sup> s<sup>-1</sup> per decade but with larger uncertainties. Note that 71% of GCMs (five CMIP6 GCMs) have negative trends, whereas only two GCMs have positive trends. The trend of dust emission fluxes induced by natural forcing is much smaller relative to GHGs and aerosols. These DAMIP results clearly indicate that increasing GHGs and anthropogenic aerosols both remarkably decrease

regional dust emission fluxes and were important drivers of recent weakening in EA dust activities.

Under different Shared Socioeconomic Pathways (SSPs), we have calculated the CMIP6 multi-model ensemble (MME) trends in dust emissions over EA according to GCMs in Supplementary Table 1. Changes of anthropogenic aerosol emissions over Asia are estimated to continue into the future, with particularly large amplitudes and large uncertainties<sup>41,47</sup>. The CMIP6 MME indicates a continuous decreasing trend during 2015–2100 in the medium-high scenario for SSP370 (Fig. 4b) and high emission scenario for SSP585 (Fig. 4c), respectively. That is mainly because high-emissions of GHGs dominated the decreasing trend of EA dust emission fluxes. Although individual GCMs have larger uncertainties for dust emission trends in SSP370 and SSP585 compared to historical simulations in Supplementary Fig. 14, these also indicate a consistent sign of trend (negative trends for five GCMs in SSP370 and SSP585). In the “middle of the road” pathway of SSP245, it indicates an increasing trend of dust emission fluxes for the near-term (2015–2050) with  $0.09 \times 10^{-10}$  kg m<sup>-2</sup> s<sup>-1</sup> in Fig. 4d, especially after 2021 ( $0.54 \times 10^{-10}$  kg m<sup>-2</sup> s<sup>-1</sup>). During the period from 2015 to 2020, the relatively high dust emissions are likely due to district change of sulfate emissions over South and East Asia<sup>41</sup>. For the long-term (2051–2100), there is a decreasing trend of dust emissions with  $-0.11 \times 10^{-10}$  kg m<sup>-2</sup> s<sup>-1</sup>. The SSP245 emission shows a sharp decline in Asian sulfate emissions during the near-term and insignificant change during the long-term<sup>47</sup>. Sharp decline of Asian sulfate emissions enhances the EA dust activities and likely dominates the increasing trend of dust emission fluxes during the near-term, whereas increasing GHGs decreases the EA dust activities during the long-term. The CMIP6 MME results show that change of EA dust activities will likely depend on emissions scenarios of GHGs and anthropogenic aerosols.

There exists a large uncertainty of the CMIP6 GCMs for regional climate change, especially for regional dust emissions<sup>48,49</sup>. Our simulated results also show a large uncertainty of dust emission fluxes for the CMIP6 GCMs in historical simulations (Fig. 4a) and in SSPs simulations (Supplementary Fig. 14). Therefore, further improvements in the dust cycle process parameterizations are needed in GCMs, which improves multiple model ensemble projection of global and regional dusts cycle.

### Concluding remarks

According to recent station observations from CMA, our results have demonstrated a significant weakening of dust activities over the EA region with Northwest China as its core since the late 1970s, which creates a strong contrast with great increase in sulfate aerosol emissions over monsoonal Asia during the same period. This study further investigated the effects of sulfate-climate interactions on EA dust activities through conducting a set of CAM4-BAM sensitivity experiments. Here, we show that anthropogenic sulfate aerosols in the Asian polluted regions significantly suppress the EA dust activities including airborne dust concentration and extreme dust events. The major processes involved for the decline in EA dust activities in response to Asian sulfate emissions are schematically summarized in Supplementary Fig. 15. The AWJS southward shift induced by Asian anthropogenic sulfate aerosols increases the precipitation through inducing low-level southwesterly wind over low latitudes, and weakens surface wind speeds through reducing the surface sensible heat flux and westerlies over mid-high latitudes. The increase in precipitation and decrease in surface wind speeds both lead to reducing the EA dust emission amounts. These aerosol-induced climate feedbacks including the AWJS southward shift, precipitation increase, and surface wind speed weakening in CAM4-BAM are reinforced by the PDRMIP multi-model simulations.

Although these idealized sensitivity simulations with Asian sulfate aerosols make a specific attribution difficult in the CAM-BAM, our results suggest that anthropogenic sulfate aerosols were a non-negligible driver of the weakened EA dust activities. The CMIP6 multi-model ensemble reinforces these sensitivity results and furtherly shows that future change of EA dust activities will likely depend on the SSPs of anthropogenic aerosols and GHGs. Compared with 1980, it shows that the mean ratios of sulfate AOD

increases are 4.0 over northern India and 2.4 over eastern China during 2013, respectively. The mean value of the ratio is almost 3 over these two regions in Supplementary Fig. 16. Based on the regional mean ratio, the climate and dust changes of increasing sulfate aerosols fall between these sensitivity experiments of SULx2Asia and SULx5Asia. The quantitative results in Fig. 4a indicate that the aerosol-induced reduction in dust emissions is  $-0.24 \times 10^{-10} \text{ kg m}^{-2} \text{ s}^{-1}$  per decade, accounting for 63% of the historical change in the all forcing simulations.

Additionally, East and South Asian sulfur dioxide emissions have been changing rapidly during recent decade with a rapid reduction in the emissions over China<sup>41</sup>. Based the MERRA-2 Reanalysis, it shows a significant decreasing trend of sulfate AOD with  $-0.053$  per decade during 2012-2018 in East Asia (also see Ref. 50) and a nearly neutral trend in South Asia in Supplementary Fig. 17a. It is noted that the frequency of observed dust storms has slightly increased with 0.99 per decade since 2012 (Supplementary Fig. 17b). This phenomenon suggests that the significant decrease in sulfate emissions over East Asia enhances dust emissions over the EA arid-semiarid region through the sulfate-climate feedbacks, which likely leads to the opposing trends of dust storm frequency and sulfate aerosols. The smaller increase in Asian dust storm frequency after 2012 may be attributed to two primary factors. First, there is a slight change of sulfate emissions over South Asia, leading to smaller change in dust storm frequency. It suggests an important influence of South Asian sulfate aerosols on East Asian (EA) dust emissions, as also supported by the sensitivity experiment (SULx10SAsia) in Supplementary Fig. 13. Second, increasing GHG emissions reduce Asian dust emissions, partially counteracting the effects of declining anthropogenic sulfate aerosol emissions.

Note that CAM4-BAM and CMIP6 simulations significantly underestimate the magnitude of the decreasing trend in EA dust activities, highly consistent with the results derived from CMIP5 simulations<sup>10</sup>. On one aspect, observational evidences show a significant dramatic recovery of vegetation coverage associated with recent wetting over the EA arid-semiarid region<sup>51</sup>, which in turn decreases the emitted-area of EA dust source and then reduces local dust emissions<sup>11,18</sup>. Due to ignoring climate-vegetation feedbacks in CAM4-BAM, our sensitivity experiments cannot show the dust reduction arising from regional vegetation recovery and thus may greatly underestimate the weakened EA dust activities induced by Asian sulfate aerosols. To eliminate the gaps between GCMs and observations in recent decline of the EA dust activities<sup>10</sup>, it is desirable to conduct more comprehensive GCM historical simulations to consider the dynamic vegetation processes together with increasing GHGs and anthropogenic aerosols in future. On the second aspect, previous studies have shown a potential impact of internal climate variability on the EA dust cycle, e.g., the North Atlantic Oscillation and the El Niño-Southern Oscillation<sup>52,53</sup>. Inability to capture the internal variability in GCMs may lead to the underestimation of the magnitude of the recent declining trend in EA dust activities<sup>54,55</sup>. Finally, previous studies show an important contribution of dust devils driven by convection to total dust emissions over North Africa during summer<sup>56</sup>. These parameterizations of dust devil emissions have been used to the numerical Weather Research and Forecast (WRF) model<sup>57</sup>. The missing parameterizations of dust devil process in GCMs may affect the changes in the East Asian dust cycle induced by Asian sulfate aerosols.

## Methods

### PDRMIP simulations

A set of idealized numerical experiments were performed to quantify the role of several climate forcings such as GHGs, solar insolation, global and regional aerosols in PDRMIP<sup>21,58</sup>. Compared with the Base experiment as fixed present-day aerosol concentrations, one perturbed experiment of regional aerosols is 10-fold increase in present-day sulfate emissions or sulfate concentrations over Asia (10°N-50°N, 60°E-140°E), labeled by SULx10Asia. Seven GCMs with SULx10Asia experiments were performed including HadGEM3-GA4, GISS-E2, IPSL-CM5A, MIROC-SPRINTARS, NCAR-CESM1-CAM4, NCAR-CESM1-CAM5, and NorESM1. In the PDRMIP simulations, a pair of numerical simulations were carried out for

15 years in forced present-day sea surface temperature (SST) simulations and for 100 years in fully coupled simulations. All the simulated data is interpolated to the same horizontal resolution with  $2.5^\circ \times 2.5^\circ$  using bilinear interpolation method. Fast response due to rapid adjustments is calculated from last 10 years in the forced SST simulations and total response (fast + slow responses) is calculated from last 50 years in the fully coupled simulations. Almost all the PDRMIP GCMs are concentration-based models, whereas MIROC-SPRINTARS and CESM1-CAM5 are emission-based models. All the PDRMIP GCMs do not predict or provide physical variables related to dust aerosols including daily surface dust mass concentration.

### CAM4-BAM description

The Community Atmosphere Model version 4 (CAM4) was the seventh generation atmospheric GCM as part of the Community Earth System Model, where the released CAM4 is the concentration-based model<sup>59</sup>. Instead of the released version, the CAM4 coupled with a bulk aerosol model parameterization (CAM4-BAM) is an emission-based one, utilizing externally mixed parameterizations and fixed size distribution of five aerosol types: dust, sea salt, organic carbon, black carbon, and sulfate<sup>59</sup> (Neale et al., 2010). The corresponding physical parameterizations of dust emission, transport, and deposition are derived from the Dust Entrainment and Deposition Model<sup>60</sup>. In CAM4-BAM, the total vertical dust flux  $F_d$  (unit:  $\text{kg m}^{-2} \text{ s}^{-1}$ ) during saltation is defined as the following formula,

$$F_d = C_{MB} \eta f_{bare} \frac{\rho}{g} u_*^3 \left( 1 - \frac{u_{*t}^2}{u_*^2} \right) \left( 1 + \frac{u_{*t}}{u_*} \right), (u_* \geq u_{*t})$$

$$F_d = 0, (u_* < u_{*t})$$

where  $C_{MB}$  is a dimensionless proportionality constant,  $g$  is the gravitational acceleration,  $\eta$  is the sand blasting efficiency, and  $\rho$  is the air density.  $f_{bare}$  is the fraction of bare soil, which decreases linearly with the leaf area index.  $u_*$  is the surface friction velocity, mainly depending on the surface wind speeds assuming neutral stability; and the threshold friction velocity  $u_{*t}$  is mostly determined by soil moisture.

The new size distribution of emitted dusts was calculated from the brittle fragmentation theory<sup>61</sup>, which is defined as relative proportion of dust mass in four size bins. This version of CAM4-BAM shows a better spatio-temporal simulation of global-scale dust aerosols and dust radiative properties<sup>62,63</sup>, which is used to investigate the EA dust cycle and the radiative feedbacks on regional climate<sup>64,65</sup>.

### CAM4-BAM numerical simulations

In this work, the CAM4-BAM utilizes the Finite-Volume (FV) dynamical core with  $192 \times 288$  output grids for horizontal resolution  $0.9 \times 1.25$  degrees and 26 levels in the vertical direction. Consistent with the PDRMIP perturbed experiments of regional anthropogenic aerosols<sup>21,58</sup>, we have carried out the Base experiment and SULx10Asia experiment (10°N-50°N, 60°E-140°E) with forced present-day SST in CAM4-BAM. The prescribed SSTs are derived from the Atmosphere Model Intercomparison Project<sup>66</sup>. The model uses the emissions of aerosols and their precursors from IPCC AR5 emissions. These fields of SST and emissions of aerosols are all at present day (typically year 2000) in all the experiments. To identify changes of the EA dust cycle induced by increasing sulfate aerosols, we have conducted two experiments with a doubling of Asian present-day sulfate emissions (SULx2Asia) and their 5-fold increase (SULx5Asia). Furthermore, two additional experiments were conducted for 10-fold increase in the present-day sulfate emissions over EA (10°N-50°N and 100°E-140°E, SULx10EAsia) and over South Asia (labeled SA, 10°N-50°N and 60°E-100°E, SULx10SAsia), respectively. These forced SST experiments from CAM4-BAM were integrated over 25 years with 5 year spin-up including the Base, SULx2Asia, SULx5Asia, SULx10Asia, SULx10EAsia, and SULx10SAsia experiments. Our model output not only includes the basic

climate variables but also dust aerosols, especially the daily surface dust mass concentration.

### Data availability

The PDRMIP dataset of numerical simulations are publicly available at: <https://cicero.oslo.no/en/projects/pdr mip>. Observational data of dust storm events from CMA are available through <http://data.cma.cn/data/cdcdetail/dataCode/A.0012.0001.S011.html>. The CMIP6 and DAMIP data are available at: <https://esgf-data.dkrz.de/search/cmip6-dkrz/>. The MERRA-2 Aerosol Reanalysis are obtained at [https://gmao.gsfc.nasa.gov/reanalysis/MERRA-2/data\\_access/](https://gmao.gsfc.nasa.gov/reanalysis/MERRA-2/data_access/). The CAM4-BAM data are available through East Asian Paleoenvironmental Science Database (<https://doi.org/10.12262/IEECAS.EAPSD2024003>).

### Code availability

Code is available from the corresponding author on reasonable request.

Received: 23 August 2024; Accepted: 19 February 2025;

Published online: 27 February 2025

### References

- Mahowald, N. M. et al. The size distribution of desert dust aerosols and its impact on the Earth system. *Aeolian Res.* **15**, 53–71 (2014).
- Miller, R. L., Knippertz, P., Pérez García-Pando, C., Perlwitz, J. P. & Tegen, I. in *Mineral Dust* (eds. Knippertz, P., Stuut, J. B.) (Springer, Dordrecht, 2014).
- Huang, J., Wang, T., Wang, W., Li, Z. & Yan, H. Climate effects of dust aerosols over East Asian arid and semiarid regions. *J. Geophys. Res. Atmos.* **119**, 11398–11416 (2014).
- Kok, J. F. et al. Mineral dust aerosol impacts on global climate and climate change. *Nat. Rev. Earth Environ.* **4**, 71–86 (2023).
- Zhang, X. Y., Arimoto, R. & An, Z. S. Dust emission from Chinese desert sources linked to variations in atmospheric circulation. *J. Geophys. Res. Atmos.* **102**, 28041–28047 (1997).
- Shao, Y. & Dong, C. H. A review on East Asian dust storm climate, modelling and monitoring. *Glob. Planet. Change* **52**, 1–22 (2006).
- Uno, I. et al. Asian dust transport one full circuit around the globe. *Nat. Geosci.* **20**, 557–560 (2009).
- Zhang, J., Peng, G., Huang, M. & Zhang, S. Are dust storm activities in North China related to arctic ice-snow cover? *Glob. Planet. Change* **52**, 225–230 (2006).
- Gong, D. Y., Mao, R. & Fan, Y. D. East Asian dust storm and weather disturbance: possible links to the Arctic Oscillation. *Int. J. Climatol.* **26**, 1379–1396 (2006).
- Wu, C. et al. Can climate models reproduce the decadal change of dust aerosol in East Asia? *Geophys. Res. Lett.* **45**, 9953–9962 (2018).
- Liu, X. D., Yin, Z.-Y., Zhang, X. Y. & Yang, X. C. Analyses of the spring dust storm frequency of northern China in relation to antecedent and concurrent wind, precipitation, vegetation, and soil moisture conditions. *J. Geophys. Res. Atmos.* **109**, D16210 (2004).
- Ding, R., Li, J., Wang, S. & Ren, F. Decadal change of the spring dust storm in northwest China and the associated atmospheric circulation. *Geophys. Res. Lett.* **32**, L02808 (2005).
- Liu, J. et al. Impact of Arctic amplification on declining spring dust events in East Asia. *Clim. Dynam.* **54**, 1913–1935 (2020).
- Wu, C., Lin, Z., Shao, Y., Liu, X. & Li, Y. Drivers of recent decline in dust activity over East Asia. *Nat. Commun.* **13**, 7105 (2022).
- Shi, Y. et al. Recent and future climate change in northwest China. *Clim. Change* **80**, 379–393 (2007).
- Peng, D. & Zhou, T. Why was the arid and semiarid northwest China getting wetter in the recent decades? *J. Geophys. Res. Atmos.* **122**, 90609–90675 (2017).
- Kraaijenbrink, P. D. A., Stigter, E. E., Yao, T. & Immerzeel, W. W. Climate change decisive for Asia's snow meltwater supply. *Nat. Clim. Change* **11**, 591–597 (2021).
- Zou, X. K. & Zhai, P. M. Relationship between vegetation coverage and spring dust storms over northern China. *J. Geophys. Res. Atmos.* **109**, D03104 (2004).
- Ramanathan, V., Crutzen, P. J., Kiehl, J. T. & Rosenfeld, D. Aerosols, climate, and the hydrological cycle. *Science* **294**, 2119–2124 (2001).
- Boucher, O. et al. *Clouds and Aerosols*. [https://www.ipcc.ch/site/assets/uploads/2018/02/WG1AR5\\_Chapter07\\_FINAL-1.pdf](https://www.ipcc.ch/site/assets/uploads/2018/02/WG1AR5_Chapter07_FINAL-1.pdf) (2013).
- Myhre, G. et al. PDRMIP: A precipitation driver and response model intercomparison project, protocol and preliminary results. *Bull. Am. Meteorol. Soc.* **98**, 1185–1198 (2017).
- Smith, S. J. et al. Anthropogenic sulfur dioxide emissions: 1850–2005. *Atmos. Chem. Phys.* **11**, 1101–1116 (2011).
- Lu, Z., Zhang, Q. & Streets, D. G. Sulfur dioxide and primary carbonaceous aerosol emissions in China and India, 1996–2010. *Atmos. Chem. Phys.* **11**, 9839–9864 (2011).
- Hoesly, R. M. et al. Historical (1750–2014) anthropogenic emissions of reactive gases and aerosols from the community emissions data system (CEDS). *Geosci. Model Dev.* **11**, 369–408 (2018).
- Aas, W. et al. Global and regional trends of atmospheric sulfur. *Sci. Rep.* **9**, 953 (2019).
- Bollasina, M. A., Ming, Y. & Ramaswamy, V. Anthropogenic aerosols and the weakening of the South Asian summer monsoon. *Science* **334**, 502–505 (2011).
- Li, Z. et al. Aerosol and monsoon climate interactions over Asia. *Rev. Geophys.* **54**, 866–929 (2016).
- Dong, B.-W., Wilcox, L., Highwood, E. & Sutton, R. Impacts of recent decadal changes in Asian aerosols on the East Asian summer monsoon: roles of aerosol-radiation and aerosol-cloud interactions. *Clim. Dynam.* **53**, 3235–3256 (2019).
- Sherman, P. et al. Sensitivity of modeled Indian monsoon to Chinese and Indian aerosol emissions. *Atmos. Chem. Phys.* **21**, 3593–3605 (2021).
- Xie, X. et al. Anthropogenic sulfate aerosol pollution in South and East Asia induces increased summer precipitation over arid Central Asia. *Commun. Earth. Environ.* **3**, 328 (2022).
- Gelaro, R. et al. The modern-era retrospective analysis for research and applications, Version 2 (MERRA-2). *J. Clim.* **30**, 5419–5454 (2017).
- Song, Z., Wang, J. & Wang, S. Quantitative classification of northeast Asian dust events. *J. Geophys. Res. Atmos.* **112**, D04211 (2007).
- Zhao, Y. et al. Impact of the middle and upper tropospheric cooling over Central Asia on the summer rainfall in the Tarim basin, China. *J. Clim.* **27**, 4721–4732 (2014).
- Peng, D., Zhou, T., Zhang, L. & Wu, B. Human contribution to the increasing summer precipitation in Central Asia from 1961 to 2013. *J. Clim.* **31**, 8005–8021 (2018).
- Dong, B., Sutton, R. T., Shaffrey, L. & Harvey, B. Recent decadal weakening of the summer Eurasian westerly jet attributable to anthropogenic aerosol emissions. *Nat. Commun.* **13**, 1148 (2022).
- Duce, R. A., Unni, C. K., Ray, B. J., Prospero, J. M. & Merrill, J. T. Long-range atmospheric transport of soil dust from Asia to the tropical North Pacific: temporal variability. *Science* **209**, 1522–1524 (1980).
- Zhao, T. L. et al. A simulated climatology of Asian dust aerosol and its trans-Pacific transport, part I: mean climate and validation. *J. Clim.* **19**, 88–103 (2006).
- Miller, R. L., Perlwitz, J. & Tegen, I. Feedback upon dust emission by dust radiative forcing through the planetary boundary layer. *J. Geophys. Res. Atmos.* **109**, D24209 (2004).
- Xie, X. et al. Radiative feedbacks of dust in snow over eastern Asia in CAM4-BAM. *Atmos. Chem. Phys.* **18**, 12683–12698 (2018).
- Xie, X. et al. Sharp decline of dust events induces regional wetting over arid and semi-arid Northwest China in the NCAR community atmosphere model. *Environ. Res. Lett.* **19**, 014061 (2024).
- Samset, B. H., Lund, M. T., Bollasina, M., Myhre, G. & Wilcox, L. Emerging Asian aerosol patterns. *Nat. Geosci.* **12**, 582–584 (2019).

42. Eyring, V. et al. Overview of the coupled model intercomparison project phase 6 (CMIP6) experimental design and organization. *Geosci. Model Dev.* **9**, 1937–1958 (2016).
43. Gillett, N. P. et al. The detection and attribution model intercomparison project (DAMIP v1.0) contribution to CMIP6. *Geosci. Model Dev.* **9**, 3685–3697 (2016).
44. Zhao, A., Ryder, C. L. & Wilcox, L. J. How well do the CMIP6 models simulate dust aerosols? *Atmos. Chem. Phys.* **22**, 2095–2119 (2022).
45. Zhao, Y. et al. Multi-model ensemble projection of the global dust cycle by the end of 21st century using the coupled model intercomparison project version 6 data. *Atmos. Chem. Phys.* **23**, 7823–7838 (2023).
46. Zhou, Y. et al. Can global warming bring more dust? *Clim. Dyn.* **61**, 2693–2715 (2023).
47. Rao, S. et al. Future air pollution in the shared socio-economic pathways. *Glob. Environ. Change* **42**, 346–358 (2017).
48. Kok, J. F., Ward, D. S., Mahowald, N. M. & Evan, A. T. Global and regional importance of the direct dust-climate feedback. *Nat. Commun.* **9**, 241 (2018).
49. Thornhill, G. et al. Climate-driven chemistry and aerosol feedbacks in CMIP6 Earth system models. *Atmos. Chem. Phys.* **21**, 1105–1126 (2021).
50. Hu, Z. et al. Temporal evolution of aerosols and their extreme events in polluted Asian regions during Terra’s 20-year observations. *Remote Sens. Environ.* **263**, 112541 (2021).
51. Li, C. et al. Drivers and impacts of changes in China’s drylands. *Nat. Rev. Earth Environ.* **2**, 858–873 (2021).
52. Zhao, Y., Huang, A., Zhu, X., Zhou, Y. & Huang, Y. The impact of the winter North Atlantic Oscillation on the frequency of spring dust storms over Tarim Basin in northwest China in the past half-century. *Environ. Res. Lett.* **8**, 024026 (2013).
53. Huang, Y., Liu, X., Yin, Z.-Y. & An, Z. Global impact of ENSO on dust activities with emphasis on the key region from the Arabian Peninsula to central Asia. *J. Geophys. Res. Atmos.* **126**, e2020JD034068 (2021).
54. Mann, M. E., Steinman, B. A. & Miller, S. K. Absence of internal multidecadal and interdecadal oscillations in climate model simulations. *Nat. Commun.* **11**, 49 (2020).
55. Smith, D. M. et al. North Atlantic climate far more predictable than models imply. *Nature* **583**, 796–800 (2020).
56. Rennó, N. O., Burkett, M. L. & Larkin, M. P. A simple thermodynamical theory for dust devils. *J. Geophys. Res. Atmos.* **55**, 3244–3252 (1998).
57. Klose, M. & Shao, Y. A numerical study on dust devils with implications to global dust budget estimates. *Aeolian Res.* **22**, 47–58 (2016).
58. Myhre, G. et al. Scientific data from precipitation driver response model intercomparison project. *Sci. Data* **9**, 123 (2022).
59. Neale, R. B. et al. *Description of the NCAR Community Atmosphere Model (CAM 4.0)*. [https://www2.cesm.ucar.edu/models/ccsm4.0/cam/docs/description/cam4\\_desc.pdf](https://www2.cesm.ucar.edu/models/ccsm4.0/cam/docs/description/cam4_desc.pdf) (2010).
60. Mahowald, N. M. et al. Change in atmospheric mineral aerosols in response to climate: last glacial period, preindustrial, modern, and doubled carbon dioxide climates. *J. Geophys. Res. Atmos.* **111**, D10202 (2006).
61. Kok, J. F. A scaling theory for the size distribution of emitted dust aerosols suggests climate models underestimate the size of the global dust cycle. *Proc. Natl Acad. Sci. USA* **108**, 1016–1021 (2011).
62. Albani, S. et al. Improved dust representation in the community atmosphere model. *J. Adv. Model. Earth Syst.* **6**, 541–570 (2014).
63. Albani, S. & Mahowald, N. M. Paleodust insights into dust impacts on climate. *J. Clim.* **32**, 7897–7913 (2019).
64. Xie, X. et al. Modeling East Asian dust and its radiative feedbacks in CAM4-BAM. *J. Geophys. Res. Atmos.* **123**, 1079–1096 (2018).
65. Wang, A., Xie, X., Liu, X. & Yin, Z.-Y. Direct radiative effect (DRE) of dust aerosols on West African and East Asian monsoon: the role of ocean-atmosphere interactions. *J. Geophys. Res. Atmos.* **127**, e2021JD035917 (2022).
66. Taylor, K. E., Williamson, D. & Zwiers F. *The Sea Surface Temperature and Sea-Ice Concentration Boundary Conditions for AMIP II Simulations*. <https://pcmdi.llnl.gov/report/ab60.html> (2000).

## Acknowledgements

This research has been supported by the National Key R&D Program of China (2023YFF0804804) and the Strategic Priority Research Program of the Chinese Academy of Sciences (XDB40030100). Xiaoning Xie is supported by the National Natural Science Foundation of China (42175059). Zhengguo Shi acknowledges the support of the Youth Innovation Promotion Association of the Chinese Academy of Sciences (Y2022101). Yangang Liu is supported by the U.S. Department of Energy’s Atmospheric System Research (ASR) program.

## Author contributions

X.N.X. and Y.L. produced the analysis of model results and wrote the original manuscript. G.M., H.Z.C., F. W., J.N.G, Z.G.S., X.Z.L., and X.D.L. assisted data analyses and contributed to the commenting of the results and revising of the manuscript.

## Competing interests

The authors declare no competing interests.

## Additional information

**Supplementary information** The online version contains supplementary material available at <https://doi.org/10.1038/s43247-025-02147-x>.

**Correspondence** and requests for materials should be addressed to Xiaoning Xie or Yangang Liu.

**Peer review information** *Communications Earth & Environment* thanks Yan Yu and the other, anonymous, reviewer(s) for their contribution to the peer review of this work. Primary Handling Editors: Kerstin Schepanski and Alice Drinkwater. A peer review file is available.

**Reprints and permissions information** is available at <http://www.nature.com/reprints>

**Publisher’s note** Springer Nature remains neutral with regard to jurisdictional claims in published maps and institutional affiliations.

**Open Access** This article is licensed under a Creative Commons Attribution-NonCommercial-NoDerivatives 4.0 International License, which permits any non-commercial use, sharing, distribution and reproduction in any medium or format, as long as you give appropriate credit to the original author(s) and the source, provide a link to the Creative Commons licence, and indicate if you modified the licensed material. You do not have permission under this licence to share adapted material derived from this article or parts of it. The images or other third party material in this article are included in the article’s Creative Commons licence, unless indicated otherwise in a credit line to the material. If material is not included in the article’s Creative Commons licence and your intended use is not permitted by statutory regulation or exceeds the permitted use, you will need to obtain permission directly from the copyright holder. To view a copy of this licence, visit <http://creativecommons.org/licenses/by-nc-nd/4.0/>.

© The Author(s) 2025